

110th Anniversary: The Dehydration and Loss of Ionic Conductivity in Anion Exchange Membranes Due to FeCl_4^- Ion Exchange and the Role of Membrane Microstructure

Michael J. McGrath,^{†,||} Nicholas Patterson,^{‡,||} Bryce C. Manubay,[†] Samantha H. Hardy,[†] John J. Malecha,[§] Zhangxing Shi,[§] Xiujun Yue,[‡] Xing Xing,[‡] Hans H. Funke,[†] Douglas L. Gin,^{§,||} Ping Liu,^{‡,||} and Richard D. Noble^{*,†,||}

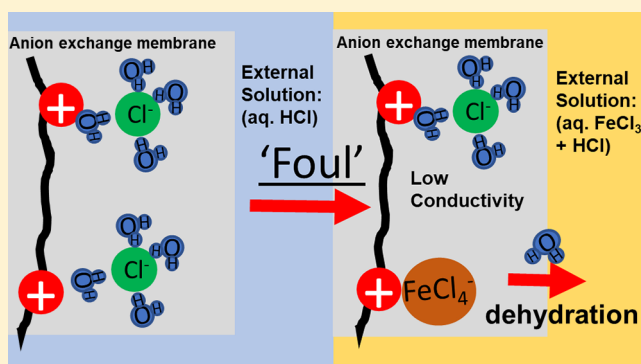
[†]Department of Chemical & Biological Engineering, University of Colorado, Boulder, Colorado 80309, United States

[‡]Department of Nanoengineering, University of California—San Diego, San Diego, California 92093, United States

[§]Department of Chemistry, University of Colorado, Boulder, Colorado 80309, United States

S Supporting Information

ABSTRACT: Anion-exchange membranes (AEMs) often dehydrate and lose ionic conductivity in ferric chloride solutions used in all-iron or iron–chromium redox flow batteries (RFB). In this work, the change in material and ionic transport properties of three AEMs with similar concentrations of ion exchange sites and hydration numbers (mol H_2O /mol ion exchange site) upon exposure to ferric chloride/hydrochloric acid solutions were studied. Raman spectroscopy and iron sorption measurements show that FeCl_4^- occupies a fraction of the AEM ion exchange sites that depends on the ferric chloride concentration in the external solution. The AEM hydration number is linearly proportional to the amount of iron sorbed in the AEMs, suggesting that the displacement of the original hydrated Cl^- counterions for unhydrated FeCl_4^- is the dominant mechanism for membrane dehydration. The ionic resistivity of the AEMs containing FeCl_4^- increased by as much as 4 orders of magnitude due to dehydration and, at high FeCl_3 solution concentrations ($\geq 1.4\text{M}$), also due to nonideal solution effects. Although the three AEMs have similar ion exchange site concentrations, the AEM with the closer local spacing of ion exchange sites exhibits higher FeCl_4^- sorption, and a correspondingly greater dehydration and resistivity increase in dilute FeCl_3 solutions.



1. INTRODUCTION

Anion exchange membranes (AEMs) exposed to ferric chloride (FeCl_3)/hydrochloric acid solutions, used in all-Fe and Fe/Cr flow batteries, rapidly lose their ionic conductivity.^{1–3} Past work by Assink et al.² showed that an AEM sorbed iron and lost up to two-thirds of its original water content, leading to a loss in ionic conductivity, and they classified this process as a form of fouling.² Assink also showed that AEMs with higher water contents maintain higher conductivities in ferric chloride solutions (e.g., foul less).³ It was proposed that sorption of anionic metal complexes could account for the significant uptake of iron into the AEMs and that these iron complexes also displace water. Iron extraction studies with ionic liquids and studies on anionic metal complex distributions inside anion-exchange resins identified the presence of FeCl_4^- .^{2,4–9} Since FeCl_4^- is poorly hydrated, it has a larger driving force compared to other anions to occupy the ion exchange sites of anion exchange resins.¹⁰ FeCl_4^- has been used to displace perchlorate anions from anion exchange resins due to its high affinity for anion exchange sites.¹⁰ However, direct evidence of

FeCl_4^- in AEMs exposed to FeCl_3/HCl solutions has not yet been reported. Furthermore, a better understanding of the factors controlling iron sorption into AEMs and its effect on AEM dehydration in FeCl_3 solutions could help design AEMs that do not lose their conductivity.

This work identifies FeCl_4^- in three AEMs (Q_1 , FAA, FAD) exposed to FeCl_3/HCl solutions by Raman spectroscopy, measures how the external FeCl_3 concentration affects this FeCl_4^- sorption, and assesses how FeCl_4^- in the AEMs affects hydration and ionic transport.

Further, a comparison of the iron sorption isotherms of the Q_1 AEM with closely spaced ion exchange sites and FAA with randomly attached ion exchange sites shows that a higher local ion exchange site concentration results in a higher AEM ion exchange selectivity for FeCl_4^- . This comparison further

Received: August 20, 2019

Revised: November 6, 2019

Accepted: November 11, 2019

Published: November 11, 2019

Table 1. Concentrations of aq. FeCl₃/HCl Solutions Used in This Study

FeCl ₃ (M)	0.0	0.2	0.4	0.6	0.8	1.0	1.2	1.4	1.5	1.6	2.0
HCl (M)	1.0	0.97	0.94	0.91	0.88	0.85	0.82	0.79	0.78	0.76	0.71

supports that ion exchange of FeCl₄⁻ is the dominant mechanism for AEM fouling in FeCl₃/HCl solutions and will provide additional information on how microstructure affects the fouling process. AEM material design strategies to prevent fouling in FeCl₃ solutions are then briefly discussed. Additionally, Assink² found that an AEM equilibrated in FeCl₃ solution rapidly recovers its conductivity when immersed in aq. HCl but offered no explanation. This work also aims to identify the changes in AEM properties during this recovery in conductivity.

2. METHODS

All error bars for measured material properties are plus or minus one sample standard deviation of at least three independent samples.

2.1. Materials. Potassium chloride (BioXtra, >99%), glycerol, radical photoinitiator (2-hydroxy-2-methyl-propio-phenone, HMP), and iron(III) chloride hexahydrate (≥98%, chunks) were purchased from Sigma-Aldrich. Both glycerol and HMP were sealed with electrical tape to prevent water absorption and HMP was stored in a 4 °C refrigerator. Standardized 0.01 N aq. silver nitrate was purchased from LabChem. All other reagents were purchased from either Sigma-Aldrich or Fischer Scientific. All reagents were used without further purification. Deionized water (<3 μS/cm) was used for preparation of solutions. Aqueous 1 M HCl and 1 M HClO₄ were diluted from 12.1 N and 70% stock solutions, respectively. Acidified FeCl₃ solutions were prepared by dilution of a 2 M FeCl₃/0.7 M aq. HCl stock solution with 1 M aq. HCl (Table 1).

The Q₁ is a highly cross-linked, dicationic bis-imidazolium based material made by the polymerization of monomer 1 and contains a periodic, phase-segregated bicontinuous cubic (*Pn3m* or *Ia3d*) pore morphology.^{11,12} Monomer 1 and the Q₁ AEM are shown in Figure 1. The size of the aqueous

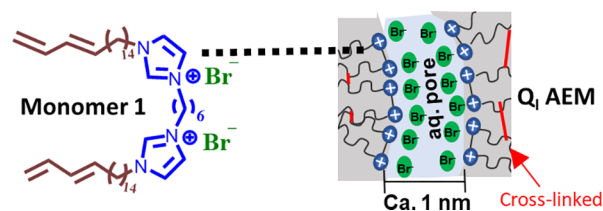


Figure 1. Schematic showing the structure of LLC monomer 1 and the Q₁ AEM formed from it that has a nanophase-separated bicontinuous cubic phase morphology.

domains in the Q₁ AEM is about 1 nm based on size-based separations of neutral solutes in nanofiltration.¹¹ LLC monomer 1 was synthesized according to previously published procedures, and its characterization data matched those previously reported.¹²

Free-standing, unsupported FAA-3 (Lot# M33161706, M35051901-1, and M35051901-2) and FAD (Sheet Lot #M32911704) AEMs with quaternary ammonium (QA) ion exchange groups were purchased from the Fuel Cell Store (College Station, TX). FAA-3 is a non-cross-linked, linear poly(arylene ether) polymer with no side chains and

trimethylammonium ion exchange groups.^{13,14} Ion and water transport have previously been studied in FAA-3 as a model AEM system.^{13–15} FAD is a QA-based AEM often used in reverse electro dialysis studies that has both high anion transport and high proton conductivity.^{16,17} No significant variation in Cl⁻ ion exchange capacity or water content for the different lots of FAA-3 used in this study was observed.

2.2. Q₁ AEM Fabrication. Thick (190–340 μm) cross-linked, Q₁ films were made following published procedures as summarized:¹¹ Monomer 1, glycerol, and HMP photoinitiator (79.4/19.8/0.8 (w/w/w)) were combined in a glass vial and hand-mixed for at least 30 min. The viscous paste was placed between two Mylar sheets and annealed for 20 min sandwiched between two 15 cm × 15 cm. × 0.6 cm fused silica plates that were squeezed together by four clamps atop a temperature-controlled hot plate (hot plate *T* = 70 °C, internal quartz plate *T* = 52.5 °C). The Mylar sheet/film sandwich was removed from the fused silica plates, cooled in ambient air for 5–10 min, and then placed again between the fused silica plates. The film/plate assembly was annealed for an additional 20 min at the same temperature (52.5 °C in-between the fused silica plates) to further equilibrate the polymer microstructure and then irradiated with 365 nm UV light (BlakRay XX40BLB) with a power density of >1 mW/cm² at the sample surface for 1 h.

The Q₁ nanostructure of the films was confirmed by powder X-ray diffraction (PXRD) (Inel CPS 120 with a Cu K_α radiation source) and polarized light microscopy (Zeiss Axioskop 40 Optical Microscope with cross polarizers) according to previous publications.^{11,12} The PXRD instrument was calibrated with silicon (NIST) and silver behenate (KODAX) powder in reflection mode. ATR FT-IR (Nicolet 6700 with a PIKE MIRacle single-reflection horizontal ATR accessory and diamond crystal) analysis confirmed a high degree of polymerization of the diene tails of monomer 1 after UV irradiation by monitoring the disappearance of the C–H out of plane wag of the 1,3-diene group on the tails at 1004 cm⁻¹.¹¹ The principal PXRD peak of the Q₁ phase varies from 2.1° to 2.3° in 2θ but all fabricated Q₁ films had a black PLM image, confirming the Q₁ structure.¹² The differences in 2θ reflect small sample-to-sample variations in the periodic order.

2.3. Membrane Resistivity Measurements. The membrane resistance was measured in a two-probe H-cell setup using electrochemical impedance spectroscopy (10 mV rms, 1 Hz–100 kHz, Gamry Reference 600). The Q₁ AEM films were first soaked repeatedly in fresh solutions of 1 M aq. HCl for a total time of at least 48 h. FAA-3 and FAD AEM films were soaked in at least one fresh solution of 1 M aq. HCl prior to exposure to an aq. FeCl₃/HCl solution of a given concentration for at least 18 h. Soaking times in 1 M aq. HCl longer than this did not affect the measured Cl⁻ ion exchange capacity, indicating that this time was sufficient to fully exchange the original Br⁻ counterions to Cl⁻. Each AEM film was only used in a single experiment.

The two-probe H-cells were assembled by clamping two L-shaped glass tubes with O-ring joints together. Each of the tubes contained a Spectracarb (2050A-1550 or 2050A-1050) carbon electrode fixed with rubber stoppers. Two flat sheet

rubber donut gaskets with 1/4 in. openings were used as seals. The impedance of the cells containing the 1 M aq. HCl or the aq. FeCl₃/HCl solution without the membranes were measured, and the resistance at high frequency was taken as the background solution resistance.

After soaking in 1 M aq. HCl, the AEM films were clamped between the donut gaskets. The more brittle Q₁ films tended to crack near the inner gasket edge in an H-cell. Therefore, Q₁ films were masked by applying Kapton tape (3D MakerWorld 0.06 mm with release liner) with 1/4 in. diameter openings on either side of the film to create a seal before loading into the H-cell (see [Supporting Information](#)). The H-cell impedance with the AEM was obtained in 1 M aq. HCl. Then the 1 M aq. HCl was replaced with the aq. FeCl₃/HCl solution at least twice within 10 min to ensure the 1 M aq. HCl solution was fully replaced by the aq. FeCl₃/HCl solution. The time-dependent change in membrane resistance was measured automatically over 24 h using the sequence function of the EIS setup. The membrane was then removed, and the aq. FeCl₃/HCl background solution resistance was measured again to assess background drift.

For AEMs exposed to aq. 2 M FeCl₃/0.7 M HCl, after 24 h the solution was fully exchanged to 1 M aq. HCl by replacing the H-cell solution at least twice to 1 M aq. HCl within 10 min. The decrease in the resistance of the fouled membranes in 1 M aq. HCl was monitored over 24 h. The background 1 M aq. HCl solution resistance was again measured to account for drifts. Further experimental details are discussed in the [Supporting Information](#).

A capacitive arc that was observed at low frequencies on Nyquist plots was associated with the carbon electrode itself (see the [Supporting Information](#)) and ignored in fitting the solution and membrane impedance. An equivalent circuit model consisting of an ideal solution resistor in series with a membrane constant phase element and membrane ideal resistor^{18,19} was used to fit the Nyquist plot data to obtain the AEM resistance. This equivalent circuit model fit merely served as a consistent way to obtain the low-frequency *x*-axis intercept of the arc associated with the fouled AEM; no attempt was made to obtain an accurate model fit of the entire Nyquist plot or interpret a physical meaning of the equivalent circuit beyond obtaining the membrane resistance.

The resistivity was calculated using [EQN 1](#):

$$R = \frac{(R_{\text{cell+membrane}} - R_{\text{cell}}) * \text{Area}}{l} \quad (1)$$

$R_{\text{cell+membrane}}$ and R_{cell} are the resistances of the cell with and without the membrane, respectively, and l is the wet membrane thickness in 1 M aq. HCl. The membrane thickness of the Q₁, FAA-3, and FAD AEMs did not differ by more than 10% across their respective membrane areas.

2.4. Ion-Exchange Capacity Determination Procedure. The AEM films were ion-exchanged with Cl⁻ counterions by soaking them in 1 M aq. KCl for at least 48 h while replacing the solution several times. The membranes were then rinsed in DI water for a total of more than 48 h to remove excess KCl from the pores, followed by successive immersion in ~10 mL of 1 M aq. KNO₃ solutions for at least 1 day each to displace the Cl⁻ counterions into the KNO₃ solutions. The Cl⁻ ion-exchange capacity (IEC) was determined by a Cl⁻ titration method of the 1 M aq. KNO₃ analyte containing the exchanged Cl⁻ ions with potentiometric indication using a Cole-Parmer Combination Cl⁻-Selective Electrode.^{20–22} A

similar methodology is described by Chen et al.²³ with colorimetric indication. The Cl⁻ IEC value was calculated using [eq 2](#) below:

$$\text{IEC} \left(\frac{\text{mmol Cl}^-}{\text{g dry AEM}} \right) = \frac{(V_{\text{AgNO}_3} * 0.01 \text{ M AgNO}_3)}{\text{mass}_{\text{dry}}} \quad (2)$$

V_{AgNO_3} is the volume of 0.01 M aq. AgNO₃ titrant at the inflection point of the titration curve, and mass_{dry} is the dry film mass with Cl⁻ counterions. Second 1 M aq. KNO₃ analytes did not contain Cl⁻ amounts above the limit of detection and therefore for some samples only the first 1 M aq. KNO₃ analyte were titrated for Cl⁻.

2.5. Water Content, Hydration Number, and Charge Density of AEMs. Wet and dry film weight measurements followed prior literature procedures.^{24–27} Wet AEM films were blotted on a KimWipe and promptly weighed on an analytical balance to obtain the wet film weight. To obtain the dry weight, films were subsequently dried under vacuum (50–80 °C, typically 1.5 h, 0.03 MPa) until their weight did not change by more than ca. 2% after >1 h of additional drying. The water content was calculated using [eq 3](#):

$$W = \frac{m_{\text{AEMwet}} - m_{\text{AEMdry}}}{m_{\text{AEMdryCl}^-}} (\text{g H}_2\text{O/g dry AEM}) \quad (3)$$

m_{AEMwet} and m_{AEMdry} are the wet and dry AEM weights, respectively, and m_{AEMdryCl^-} is the dry, unfouled AEM mass with Cl⁻ counterions.

The hydration number is subsequently given by [eq 4](#):

$$\lambda = \frac{1000 * (W/18.02)}{\text{IEC}} \quad (4)$$

As a first-order approximation, the water volume fraction is assumed equal to the water content, assuming a water density of 1 g/cm³, and the fixed charge concentration was calculated as^{28,29}

$$C_{\text{fix}} = \frac{\text{IEC}}{W/\rho} \quad (5)$$

IEC is the Cl⁻ ion exchange capacity from [eq 2](#), W is the g H₂O/g dry sample from [eq 3](#), and ρ is the density of water (1 g/cm³).

2.6. Raman Spectroscopy. Raman spectra (DXR Microscope, USA) were measured at room temperature using a 1200 grating and 10 s exposure time from 105 to 1300 cm⁻¹. Background spectra of the aq. FeCl₃/HCl solutions were obtained with small aliquots pipetted onto glass slides and covered with optical-grade glass cover slides. Q₁, FAA-3, and FAD AEMs were soaked in the same FeCl₃/HCl solutions for a minimum of 2 weeks for equilibration. The equilibrated AEMs were then removed from the solutions, and the surfaces were blotted to remove excess solution before being placed on a glass microscope slide. A cover slide was then placed on top of the AEMs before the collection of the spectra.

2.7. Equilibrium Iron Sorption and AEM Stability Assessment. Three AEM films (20–50 mg) were soaked several times in fresh 1 M aq. KCl solutions for a total time of several days, then soaked twice in DI water (for total of >1 day), and dried under vacuum (50–80 °C, typically 1.5–8 h, 0.03 MPa) to obtain the dry sample mass. The AEM films were then soaked in 1 M aq. HCl for at least 2 days, followed by immersion in >10 mL of a given aq. FeCl₃/HCl solution for at

Table 2. Material Properties of AEMs in This Study

AEM ^a	Structure	Ion Exchange Group	Water Content (g H ₂ O g ⁻¹)	Cl ⁻ IEC (mmol g ⁻¹)	C _{fix} (mol L ⁻¹)	Area% Swelling in DI Water	Conductivity in 1M aq. HCl (mS/cm)
Q ₁	Phase-segregated	Imidazolium	0.30 ± 0.04	2.3 ± 0.2	8 ± 1	24 ± 4	9 ± 2
FAA-3	Amorphous	-N(CH ₃) ₃ ⁺	0.24 ± 0.02	1.9 ± 0.2	8 ± 1	23 ± 2	7 ± 3
FAD	Amorphous	QA ^b	0.28 ± 0.02	1.92 ± 0.02	6.9 ± 0.5	25 ± 3	14 ± 2

^aAll AEMs are unsupported, freestanding films. ^bIon exchange group unknown but likely QA (quaternary ammonium) based on ref 33.

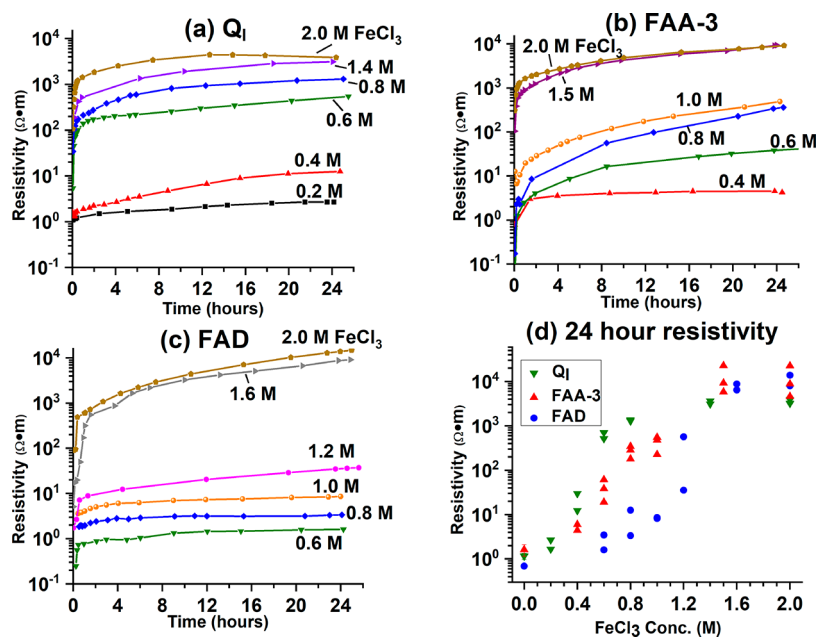


Figure 2. AEM resistivity as a function of time exposed to FeCl₃/HCl solutions of various concentrations for the (a) Q₁, (c) FAA-3, (c) FAD AEMs, and (d) the AEM resistivity after 24 h for all tested samples. HCl solution concentrations varied with FeCl₃ concentrations according to Table 1.

least 10 days to reach equilibrium. The amount of sorbed iron did not increase when the soaking time was increased from 10 to 18 days at all FeCl₃ concentrations used, suggesting complete equilibration after 10 days. The equilibrated AEM samples were removed from the FeCl₃/HCl solutions, blotted dry with Kim wipes, and placed in an ~10 mL aliquot of 1 M aq. HCl to extract the iron. Several more extractions were performed over several days in this same manner until no iron was detected in the extract solution. Typically, no iron was detected after a single 48-h extraction. The 1 M aq. HCl extract was diluted, and its UV–vis absorbance at 335 nm was measured with an Agilent 8453 UV–vis spectrometer. A calibration curve was used to quantify the amount of extractable iron in the AEM. The sum of iron from successive extractions was normalized by the original AEM sample mass (in Cl⁻ counterion form). The fraction of total ion exchange sites occupied by iron was calculated according to eq 6:

$$\theta = \frac{(\text{mmol Fe extracted/g dry AEM})}{\text{IEC}} \quad (6)$$

AEM Stability in FeCl₃ Solutions. The dry sample masses of the AEMs with Cl⁻ counterions after iron extraction with 1 M aq. HCl were obtained after rinsing the samples in DI water to remove residual acid and drying them under vacuum (50–80 °C, typically 3–8 h, 0.03 MPa). The dry mass of all samples, as well as the ATR FT-IR spectra and IEC for a subset of these samples, were compared to the original values before exposure

to aq. FeCl₃/HCl solutions to assess stability (see Supporting Information).

2.8. AEM Water Content in Ferric Chloride Solutions. The same pretreatment steps, dry sample mass measurement, and iron solution equilibration steps as those used for the iron sorption experiment (Section 2.7) were carried out on three different AEM samples in each aq. FeCl₃/HCl solution. The water content was then obtained as described in Section 2.5.

2.9. Area % Swelling. The area % swelling was calculated according to eq 7. The areas were determined from images of the film sandwiched between two microscope slides with ruler graduations using ImageJ software, similar to other published procedures.³⁰ Wet film areas were obtained with the solutions imbibed between the microscope slides, and dry film areas were determined directly after removal of the samples from the vacuum oven (50–80 °C, typically 1.5–8 h, 0.03 MPa). Thickness % swelling measurements^{23,31} were less accurate because the film thicknesses varied, and it was difficult to measure the thickness of the same exact spot on the film before and after drying.

$$\text{Area \% Swelling} = \frac{\text{Area}_{\text{wet}} - \text{Area}_{\text{dry}}}{\text{Area}_{\text{dry}}} \quad (7)$$

2.10. Swelling Kinetics of Fouled AEMs in 1 M aq. HCl. AEMs with Cl⁻ counterions were soaked in aq. 2 M FeCl₃/0.7 M HCl solution for 24 h. The samples were then placed between two graduated glass slides, imbibed with aq. 2

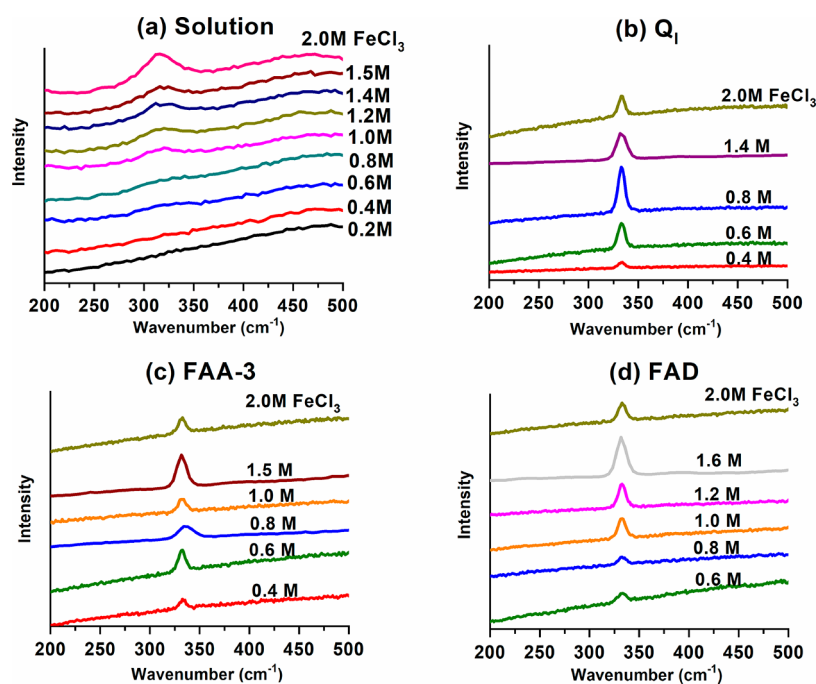


Figure 3. Raman spectroscopy of (a) FeCl_3/HCl solutions and (b) Q_1 , (c) FAA-3, and (d) FAD AEMs equilibrated with the same FeCl_3/HCl solutions. HCl solution concentrations varied with FeCl_3 concentrations according to Table 1.

M $\text{FeCl}_3/0.7$ M HCl , and imaged. After removal of excess solution using KimWipes, the samples were then soaked in 1 M aq. HCl for 24 h and periodically removed from the soaking solution for imaging according to Section 2.9.

3. RESULTS AND DISCUSSION

3.1. AEM Properties. Table 2 summarizes the ionic properties of the three AEMs investigated (Q_1 , FAA-3, and FAD). The Cl^- IEC value for FAA-3 is in reasonable agreement with that reported by Marino (2.1 mmol Cl^-/g).¹³ The IEC value for FAD is similar to that reported by the manufacturer¹⁷ but much higher than that found by Dlugolecki (0.13 mmol Cl^-/g) despite similar procedures.¹⁶ The measured water content of FAD is much lower than that reported by the manufacturer (58 wt %).¹⁷ SAXS of the AEMs in the as-made dry state (Br^- counterion) confirms the Q_1 phase morphology of the Q_1 AEM and the lack of order in the FAA-3 and FAD membranes (see the Supporting Information). Only diffuse order for FAA-3 by SAXS was observed by Marino.¹³ The higher conductivity of FAD than Q_1 or FAA is likely related to its high proton conductivity as reported by the manufacturer.¹⁷ Dlugolecki reported that FAD contains both strongly basic and weakly acidic ion exchange groups.^{16,32} The weakly acidic ion exchange groups would be the source of H^+ ions which would provide high conductivity. However, the ion exchange capacity of FAD measured in this study using both 1 M aq. KCl and 1 M aq. HCl as the solution used to introduce Cl^- counterions were similar and much higher than the ion exchange capacity found by Dlugolecki.^{16,32} Therefore, no evidence for weakly acidic functional groups in the FAD samples tested in this work was found.

The Q_1 , FAA, and FAD AEMs equilibrated in the FeCl_3/HCl solutions were chemically stable (see Section 2.7 and Supporting Information).

3.2. Fouling Kinetics. The resistivities of all three AEMs (Q_1 , FAD, and FAA-3) increase after exposure to the $\text{FeCl}_3/$

HCl solutions and to a greater extent with higher FeCl_3 concentrations. A single capacitive arc on Nyquist plots for AEMs exposed to sufficiently concentrated FeCl_3 solutions can be assigned to impedance within the membrane, likely due to dehydration-induced heterogeneous transport³⁴ and not due to a surface foulant layer (see Supporting Information). This finding agrees with that of Assink, who found no evidence of a surface foulant layer by SEM-electron microprobe analysis.² Some examples of the time dependency of these increases are shown in Figure 2 (see Supporting Information for all samples tested), as well as the resistivity of all samples after 24 h of exposure to the FeCl_3/HCl solutions.

Even though the AEM resistivities did not reach equilibrium after 24 h of solution exposure, equilibration was sufficiently close for comparison of AEM resistivities across different FeCl_3/HCl solutions. The resistivity of the Q_1 AEM increased more than those of the FAA-3 and FAD AEMs in more dilute FeCl_3 solutions, as shown in Figure 2d. For each AEM, the resistivity increased by about 4 orders of magnitude and reached a similar limiting value at the highest FeCl_3 concentrations.

3.3. Identification of FeCl_4^- in AEMs by Raman Spectroscopy. The Raman spectra of aq. FeCl_3/HCl solutions and of the three AEMs equilibrated in the same solutions are compared in Figure 3. In solution, a singular, diffuse peak at 317 cm^{-1} increases with FeCl_3 concentration. This peak is consistent with that of $\text{Fe}(\text{H}_2\text{O})_2\text{Cl}_2^+$.³⁵ This is expected to be the dominant iron-containing species in these solutions.³⁶ A broad feature at 260 cm^{-1} associated with Fe_2Cl_7^- is only detectable in the 2 M aq. FeCl_3 solution.³⁷ Peaks of other ferric species were not detected in the Raman spectra. A sharp, polarized peak at 331 cm^{-1} exists in the spectra of all AEMs exposed to aq. FeCl_3/HCl solutions. This peak is consistent with the formation of the anionic complex FeCl_4^- .^{10,38} These observations are consistent with an ion-exchange process (eq 8) of FeCl_4^- into the AEMs, as suggested

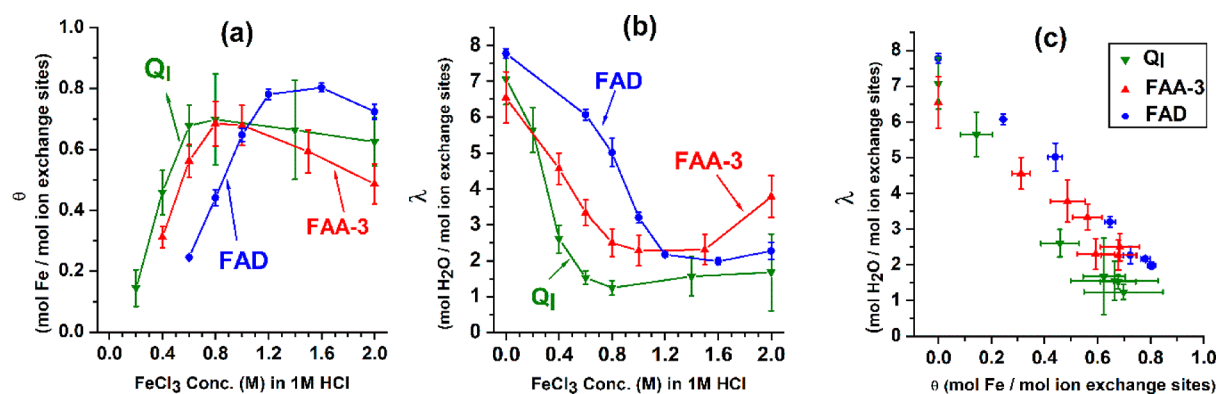
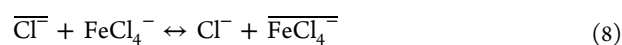


Figure 4. (a) Iron sorption as a fraction, Θ , of total accessible ion exchange sites, (b) hydration number (mol H₂O per mol of ion exchange sites), and (c) hydration number as a function of the iron sorption, Θ , for the Q₁, FAA-3, and FAD AEMs exposed to different aq. FeCl₃/HCl solutions. HCl solution concentrations varied with FeCl₃ concentrations according to Table 1.

by Assink^{2,3} and Reiner.³⁹ Anion exchange of metal-halide complexes into anion exchange resins is well-known and is used in the chromatographic separations of metals.^{40,41} The presence of the strong FeCl₄⁻ Raman signals in each of the AEMs suggests that most of the iron sorbs as FeCl₄⁻ counterions at the ion exchange sites. The high concentration of halide ligands and low dielectric constant in the pores of anion-exchange resins also strongly favor high coordination number, negatively charged metal-halide complexes such as FeCl₄⁻.^{7,40,41} Similarly, FeCl₄⁻ concentrations increase in solutions with increasing Cl/Fe ratio and in lower dielectric solvents.^{10,35,36} These factors promote either the speciation of sorbed (FeCl_xⁿ⁺ + n Cl⁻) salt pairs into FeCl₄⁻ inside the AEM or the direct ion exchange of FeCl₄⁻ from solution into the AEMs.



Overbars denote the counterion at an AEM ion exchange site in eq 8.

3.4. Equilibrium Iron and Hydration Number of AEMs in FeCl₃ Solutions. The equilibrium amount of iron sorbed in the AEM (as a fraction of the total accessible ion exchange sites) is shown as a function of the external FeCl₃ concentration in Figure 4a. The iron sorption increases for all three AEMs with increasing FeCl₃ concentration and then decreases slightly (for the Q₁ and FAD) or substantially (for FAA-3) at higher FeCl₃ concentrations in solution. Such behavior is commonly observed for ion exchange of anionic metal complexes into anion exchange resins.⁴⁰ The decrease in iron sorption at higher FeCl₃ concentrations likely reflects a lower ion exchange site selectivity for FeCl₄⁻ over Cl⁻ (see eq 8), due to difficult-to-predict changes in ion activities in the AEMs and in solution.⁴⁰ If all sorbed iron is assumed to be FeCl₄⁻ at ion-exchange sites, a maximum of (70 ± 20)%, (68 ± 7)%, and (80 ± 1)% of IEC sites are taken up by iron in the Q₁ (at 0.8 M aq. FeCl₃ in solution), FAA-3 (at 0.8 and 1 M aq. FeCl₃), and FAD (at 1.6 M aq. FeCl₃) AEMs, respectively. The high iron sorption into the AEMs agrees with the work of Assink et al.,² who showed that 74% of the IEC sites of an AEM were taken up by iron when exposed to an aq. 2 M FeCl₃/1 M HCl solution.

The amount of sorbed iron shown in Figure 4a was determined by extracting equilibrated samples with 1 M aq. HCl; thus, the contribution of insoluble iron hydroxides to the total sorption is likely insignificant. Additionally, such insoluble

species would not be stable in the low pH of the solutions (pH < 0). Further, even though the samples loaded with iron are dark orange, they turn colorless after extraction, suggesting the absence of iron hydroxides in the AEM pores.

As shown in Figure 4b, the hydration number of each of the AEMs drops significantly with increasing FeCl₃ solution concentration but then increases slightly (for the Q₁ and FAD) or substantially (for FAA-3) at sufficiently high FeCl₃ concentrations. The hydration numbers of AEMs depend both on the difference in water activity of the external solution and inside the AEM and on the hydration of the counterion.⁴² Since FeCl₄⁻ is likely unhydrated based on Raman studies^{35,38} and extraction measurements from water into hydrophobic ionic liquids,^{4,9} the hydration numbers of the AEMs are expected to decrease with increasing FeCl₄⁻ sorption. As shown in Figure 4c, the hydration numbers of the AEMs decrease linearly with the amount of sorbed iron, regardless of the external FeCl₃ solution concentration. This information suggests that dehydration mainly occurs due to FeCl₄⁻ ion exchange and not due to a lowering of the external solution's water activity with increasing FeCl₃ concentration (e.g., osmotic dehydration^{2,42,43}). Furthermore, water content measurements on the AEMs exposed to aq. LiCl solutions with the same water activities as the FeCl₃ solutions show that loss of water due to a lowering of the water activity in the high ionic strength FeCl₃ solutions plays a lesser role than dehydration due to FeCl₄⁻ sorption (see Supporting Information).

3.5. AEM Resistivity Dependence on Hydration State of AEM. As shown in Figure 5, the resistivities of the Q₁ and FAA-3 AEMs after 24 h of exposure to dilute FeCl₃ solution increased with decreasing hydration number (0.2–0.8 M aq. FeCl₃ for the Q₁ and 0.4–1 M aq. FeCl₃ for FAA-3). The resistivity of FAD did not show a clear dependence on hydration number (within the experimental accuracy), possibly due to the high proton conductivity of FAD. However, even though the hydration numbers increase slightly (for Q₁ and FAD) or significantly (for FAA-3) at the high FeCl₃ concentrations (for Q₁ ≥ 1.4 M, FAA-3 at 2 M aq. FeCl₃, and FAD ≥ 1.6 M), the membrane resistivities further increase, suggesting that the hydration number is not the only factor that affects ion transport resistances. Water in AEMs typically controls the extent of percolated pathways for ion transport and also dissociates ions from each other to increase their mobility.^{3,13,34} Assink showed that the resistivity depended on

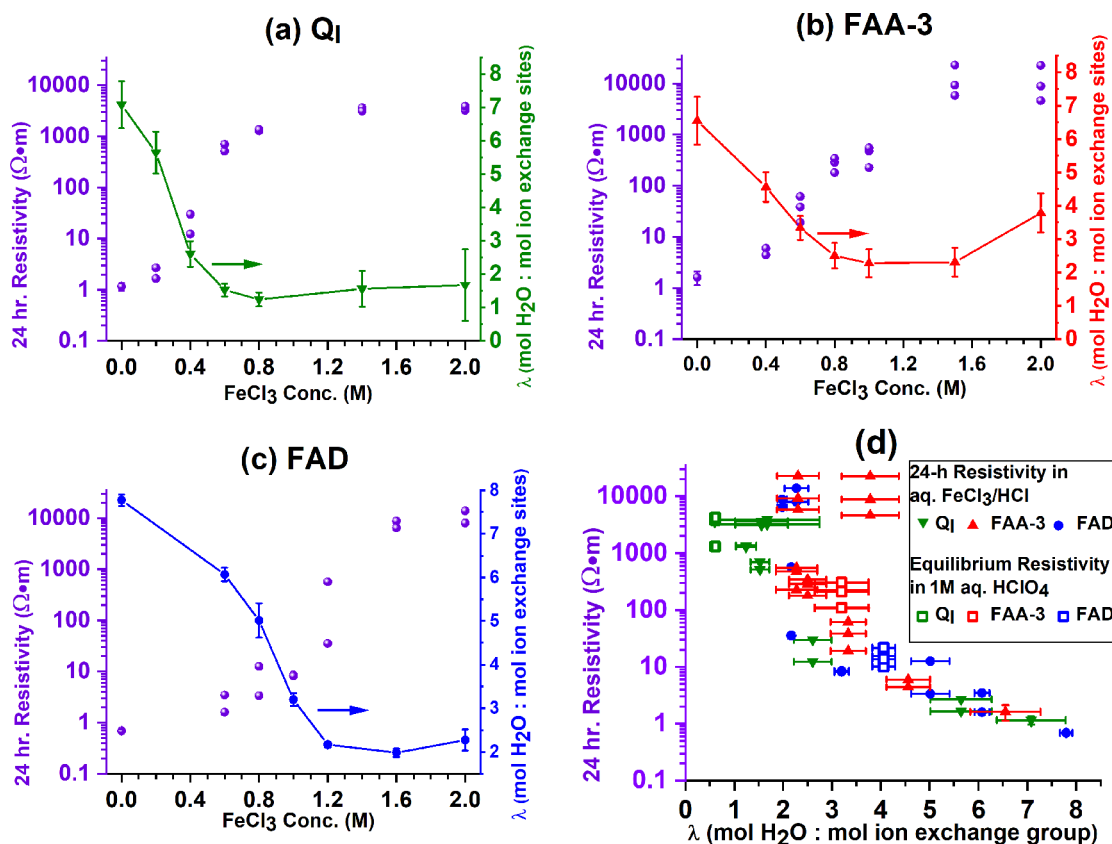


Figure 5. Resistivity after 24 h and equilibrium hydration number versus external FeCl₃ concentration for (a) Q₁, (b) FAA-3, and (c) FAD AEMs and (d) resistivities as a function of equilibrium hydration number for each individually tested AEM sample. HCl solution concentrations varied with FeCl₃ concentrations according to Table 1.

the water content according to percolation theory.² The water content and the resistivities of the AEMs in this study are often well below or above, respectively, those of the AEM studied by Assink² (<0.08 g H₂O/g dry polymer and 3000–22 000 Ω·m in 2 M aq. FeCl₃ solutions here versus 0.2 g H₂O/g dry polymer and 100 Ω·m by Assink). Thus, ion pairing and, consequently, low ion mobility in the AEMs could play a more significant role here.

The changes in resistivity and hydration number of the AEMs when exchanged to the poorly hydrated^{10,40,44–46} perchlorate (ClO₄⁻) counterions of similar size to Cl⁻ (Stokes radius⁴⁷ for Cl⁻ of 1.21 Å vs 1.35 Å for ClO₄⁻) were measured to help identify the role of the hydration state of the counterion on the resistivity without complicating effects from FeCl₃ solutions, such as osmotic dehydration or nonspecific sorption of FeCl_xⁿ⁺ + n Cl⁻ salt pairs. The Q₁ resistivity in 1 M aq. HClO₄ is comparable to that in aq. 2 M FeCl₃/0.7 M aq. HCl (see Figure 5d) suggesting that the presence of a poorly hydrated counterion, whether ClO₄⁻ or FeCl₄⁻, leads to low hydration, significant ion binding, and consequently a high ion transport resistance in the Q₁ AEM. The resistivities of FAA-3 and FAD were higher in 1 M aq. HClO₄ than in 1 M aq. HCl likely due to the presence of the poorly hydrated ClO₄⁻ counterion, but the extent of dehydration and increase in resistivity are less than in the case of the Q₁ AEM. The resistivities of FAA and FAD in concentrated FeCl₃ (>1.5M) solutions are much higher than in 1 M aq. HClO₄. This suggests that nonideal effects, such as lower water activity coefficients and a lesser ability for water to keep ions solvated in the AEM (see Supporting Information Section VII), or

sorption of low mobility (FeCl_xⁿ⁺ + n Cl⁻) salt pairs that occupy free-volume, are needed in combination with ion exchange of an unhydrated anion (e.g., FeCl₄⁻), to afford the very high resistivities observed for FAA-3 and FAD in concentrated FeCl₃ solutions.

3.6. Role of Local Ion Exchange Site Concentration on the Sorption of FeCl₄⁻. As shown in Figure 4, the Q₁ AEM more readily sorbs iron from dilute FeCl₃/HCl solutions than FAA-3 or FAD, most likely as FeCl₄⁻ (Section 3.3). A higher ion exchange site concentration means a higher concentration of Cl⁻ counterions that can serve as ligands to iron, and thus favors FeCl₄⁻ sorption.^{7,40,41} Further, the hydrophilic domains of AEMs are highly charged and confined within the AEM polymer matrix. The electric fields that arise from the charged ion exchange sites in an AEM align the water molecules, lower the dielectric constant, and thus decrease solvation of the counterions, resulting in a higher ion-exchange selectivity for less hydrated counterions (such as FeCl₄⁻) over more hydrated counterions (Cl⁻).⁴⁸ Additionally, higher charge densities inside the AEM favor more ion binding with the ion exchange sites^{13,28,49} leading to a loss in water,^{13,50,51} which also leads to a greater selectivity for less hydrated counterions.

The average fixed charge concentrations (and Cl⁻ ligand concentration) of the Q₁, FAA-3, and FAD AEMs are similar (see Table 1). However, the local concentration of charge and Cl⁻ ligands for the Q₁ AEM are likely higher, due to the close proximity of the bis-imidazolium ion exchange sites on the head group of monomer 1 (see Figure 1) and their localization in ca. 1 nm phase-segregated domains, resulting in a high ion-

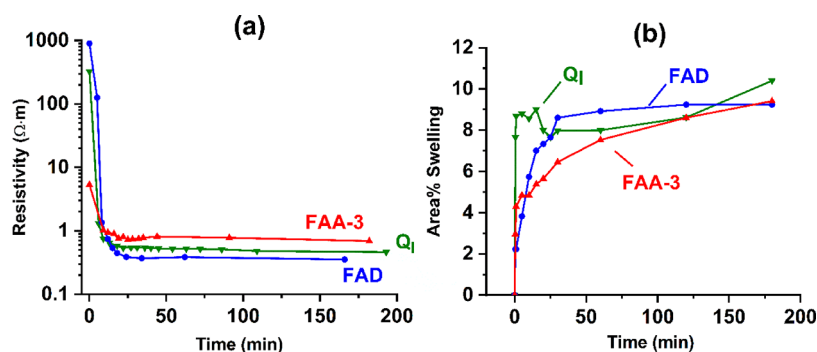


Figure 6. (a) Resistivity decrease and (b) swelling increase of AEMs versus time exposed to 1 M aq. HCl after 24 h exposure to 2 M aq. $\text{FeCl}_3/0.7$ M aq. HCl.

exchange selectivity for unhydrated FeCl_4^- over more hydrated Cl^- . FAA-3 has an amorphous structure by SAXS,¹³ suggesting that the trimethylammonium groups on FAA-3 are randomly distributed,^{13,51} resulting in a lower local ion exchange site concentration than in the Q_1 AEM and therefore lower selectivity for FeCl_4^- . Further, larger aqueous domains with a higher dielectric constant (due to lower local ion exchange site concentration) that can better solvate Cl^- may be present in the FAA-3 and FAD pores, translating into a lower selectivity for FeCl_4^- .

The higher selectivity of the imidazolium-based Q_1 AEM for FeCl_4^- compared to quaternary ammonium (QA)-based FAA-3 and FAD is likely not due to differences in the ion exchange group itself. Weiber et al.⁵¹ found that Br^- counterions more readily associate with trimethylammonium groups than imidazolium ion exchange groups appended to the same polymer backbone. If this finding also holds for FeCl_4^- counterions, less binding to imidazolium groups would result in a lower, not higher, selectivity for FeCl_4^- . Further, the Raman Fe–Cl stretch frequency of FeCl_4^- does not differ between the AEMs, indicating the strength of interaction with the ion exchange sites is the same. ATR FT-IR and Raman analyses of model ionic liquids further support that hydrogen bonding, present in imidazolium ion exchange groups, is not significant with FeCl_4^- (see Supporting Information).

Other differences in the AEM properties besides local ion exchange site concentration that determine hydration near the ion exchange sites, and therefore the tendency to bind ions and expel water, could also affect the selectivity for FeCl_4^- over Cl^- . These factors include the overall water content, hydrophilicity of the polymer backbone, and the relative importance of osmotic dehydration. Therefore, the role of the local ion exchange site concentration versus these other factors in determining the sorption of FeCl_4^- is not conclusive but likely plays an important part.

3.7. Design of AEMs to Prevent FeCl_4^- Sorption. Size exclusion of FeCl_4^- from the aqueous AEM domains would be difficult to achieve in these flexible, polymeric AEMs since the ion sizes are very small (i.e., Stokes radius of 1.21 and 3.1 Å for Cl^- ⁴⁷ and FeCl_4^- ⁵², respectively). The high Cl^- ligand concentration in the AEMs and the unhydrated nature of FeCl_4^- create a strong driving force for ion exchange of FeCl_4^- into the AEMs, making ion size a difficult driver for selectivity. Smaller aqueous domains can increase the selectivity for FeCl_4^- , ion binding, and AEM dehydration since the charge density in the AEM is higher. Instead of tuning the size of the entire aqueous domain, adding bulky side groups to the ion-exchange sites to sterically prevent FeCl_4^- from binding to

them is a more promising approach to minimize AEM fouling in FeCl_3/HCl solutions, as suggested by Reiner.³⁹

3.8. Recovery of Fouled AEMs in 1 M aq. HCl. AEMs exposed to aq. 2 M $\text{FeCl}_3/0.7$ M HCl for 24 h that are then exposed to aq. 1 M HCl show a rapid decrease in their resistivity and swell rapidly (Figure 6). The resistivity of each AEM decreases by over 80% within 10 min of exposure to 1 M aq. HCl. Gu reported facile displacement of FeCl_4^- from anion exchange resins by exposing the resins to dilute aq. HCl. Gu states that this facile displacement is due to the decomposition of FeCl_4^- into positively charged Fe(III) species that are readily desorbed from the resin by charge repulsion.¹⁰ In this work, the iron desorption kinetics and Raman spectra of the fouled AEMs after exposure to 1 M aq. HCl were not measured to assess whether FeCl_4^- inside the AEM forms into other iron species or desorbs rapidly. It is also possible that water uptake into the AEMs and the swelling of the AEM hydrophilic domains may cause the resistivity to decrease even before the iron has been extracted from the membrane. A percolation model would predict resistivity of the AEMs to rapidly decrease upon reaching a critical water volume fraction θ_c ^{2,53,54} upon swelling in 1 M aq. HCl. The swollen hydrophilic domains may allow for transport of H^+ or Cl^- , resulting in recovery of conductivity. It is also possible that the FeCl_4^- anion becomes more mobile upon water uptake of the membrane, as the size of conductive domains is known to enhance diffusion of large species disproportionately to smaller species.⁵⁵

CONCLUSIONS

Raman spectroscopy and equilibrium iron sorption measurements on three different anion exchange membranes (AEMs) show that iron readily sorbs into the AEMs from FeCl_3/HCl solutions as FeCl_4^- , directly confirming the suggestions of past work.^{2,3,39} Because FeCl_4^- is unhydrated and displaces the original, more hydrated Cl^- counterions, the AEM hydration number decreases linearly with the amount of iron sorbed. An AEM (Q_1) with closer spacing of ion exchange sites more readily sorbs FeCl_4^- from dilute (≤ 0.6 M) FeCl_3 solutions than two amorphous AEMs (FAA-3 and FAD) with similar overall fixed concentration of ion exchange sites and hydration numbers. As a result, in more dilute FeCl_3 solutions the dehydration and resistivity increase of the Q_1 AEM are greater than those for FAA-3 and FAD.

In sufficiently dilute FeCl_3 solutions (< 1.2 M), the resistivity of each AEM increases while the hydration number decreases. However, at higher FeCl_3 concentrations (e.g., 1.4–2.0 M

FeCl₃), the resistivities continue to increase, even though the sorbed iron in each AEM decreases and the hydration number slightly increases. Lower water activity inside the AEM and higher sorption of (FeCl_xⁿ⁺ + n Cl⁻) salt pairs and associated increase in ionic binding might explain the lower ionic mobility in more concentrated FeCl₃ solutions.

■ ASSOCIATED CONTENT

📄 Supporting Information

The Supporting Information is available free of charge at <https://pubs.acs.org/doi/10.1021/acs.iecr.9b04592>.

SAXS spectra, AEM stability data (mass change, ion exchange capacity, ATR FT-IR) in ferric chloride solutions, iron sorption results by sample mass analysis, resistivity versus time curves for all samples, Nyquist plots, solution conductivities, water content measurements in aq. LiCl solutions, swelling recovery kinetics curves for all samples, calculations of material properties from literature references, more detailed descriptions for material characterization methods, Raman control studies of imidazolium ionic liquids (PDF)

■ AUTHOR INFORMATION

Corresponding Author

*E-mail: richard.noble@colorado.edu.

ORCID

Michael J. McGrath: 0000-0002-3432-2767

Nicholas Patterson: 0000-0001-7271-692X

Douglas L. Gin: 0000-0002-6215-668X

Ping Liu: 0000-0002-1488-1668

Richard D. Noble: 0000-0002-2712-3700

Present Address

Zhangxing Shi: Argonne National Laboratory, 9700 S Cass Ave., Lemont, IL 60439. Xiujun Yue: Department of Mech. Eng. and Applied Mechanics, Univ. of Pennsylvania.

Author Contributions

[†]M.J.M. and N.P. contributed equally to this work.

Funding

Primary financial support for this work was provided by the U.S. DOE ARPA-E program (grant: DE-AR0000770).

Notes

The authors declare no competing financial interest.

■ REFERENCES

- (1) Dinesh, A.; Olivera, S.; Venkatesh, K.; Santosh, M. S.; Priya, M. G.; Inamuddin; Asiri, A. M.; Muralidhara, H. B. Iron-Based Flow Batteries to Store Renewable Energies. *Environ. Chem. Lett.* **2018**, *16* (3), 683–694.
- (2) Assink, R. A. Fouling Mechanism of Separator Membranes for the Iron/Chromium Redox Battery. *J. Membr. Sci.* **1984**, *17* (2), 205–217.
- (3) Arnold, C.; Assink, R. A. Structure–Property Relationships of Anionic Exchange Membranes for Fe/Cr Redox Storage Batteries. *J. Appl. Polym. Sci.* **1984**, *29* (7), 2317–2330.
- (4) Vander Hoogerstraete, T.; Wellens, S.; Verachtert, K.; Binnemans, K. Removal of Transition Metals from Rare Earths by Solvent Extraction with an Undiluted Phosphonium Ionic Liquid: Separations Relevant to Rare-Earth Magnet Recycling. *Green Chem.* **2013**, *15* (4), 919.
- (5) Wang, J.; Yao, H.; Nie, Y.; Bai, L.; Zhang, X.; Li, J. Application of Iron-Containing Magnetic Ionic Liquids in Extraction Process of Coal

Direct Liquefaction Residues. *Ind. Eng. Chem. Res.* **2012**, *51* (9), 3776–3782.

(6) Visser, A. E.; Swatloski, R. P.; Griffin, S. T.; Hartman, D. H.; Rogers, R. D. Liquid/Liquid Extraction of Metal Ions in Room Temperature Ionic Liquids. *Sep. Sci. Technol.* **2001**, *36* (5–6), 785–804.

(7) Marcus, Y. The Anion Exchange of Metal Complexes—IV The Iron(III)-Chloride System. *J. Inorg. Nucl. Chem.* **1960**, *12* (3–4), 287–296.

(8) Rutner, E. The Reflectance Spectra of Chlorocobaltous and Chloroferri Complex Ions on Dowex-1 Anion-Exchange Resin. *J. Phys. Chem.* **1961**, *65* (6), 1027–1030.

(9) Kogelnig, D.; Stojanovic, A.; Jirsa, F.; Körner, W.; Krachler, R.; Keppler, B. K. Transport and Separation of Iron(III) from Nickel(II) with the Ionic Liquid Trihexyl(Tetradecyl)Phosphonium Chloride. *Sep. Purif. Technol.* **2010**, *72* (1), 56–60.

(10) Gu, B.; Brown, G. M.; Maya, L.; Lance, M. J.; Moyer, B. A. Regeneration of Perchlorate (ClO₄⁻)-Loaded Anion Exchange Resins by a Novel Tetrachloroferrate (FeCl₄⁻) Displacement Technique. *Environ. Sci. Technol.* **2001**, *35* (16), 3363–3368.

(11) Carter, B. M.; Wiesenauer, B. R.; Hatakeyama, E. S.; Barton, J. L.; Noble, R. D.; Gin, D. L. Glycerol-Based Bicontinuous Cubic Lyotropic Liquid Crystal Monomer System for the Fabrication of Thin-Film Membranes with Uniform Nanopores. *Chem. Mater.* **2012**, *24* (21), 4005–4007.

(12) Dischinger, S. M.; McGrath, M. J.; Bourland, K. R.; Noble, R. D.; Gin, D. L. Effect of Post-Polymerization Anion-Exchange on the Rejection of Uncharged Aqueous Solutes in Nanoporous, Ionic, Lyotropic Liquid Crystal Polymer Membranes. *J. Membr. Sci.* **2017**, *529*, 72–79.

(13) Marino, M. G.; Melchior, J. P.; Wohlfarth, A.; Kreuer, K. D. Hydroxide, Halide and Water Transport in a Model Anion Exchange Membrane. *J. Membr. Sci.* **2014**, *464*, 61–71.

(14) Münchinger, A.; Kreuer, K.-D. Selective Ion Transport through Hydrated Cation and Anion Exchange Membranes I. The Effect of Specific Interactions. *J. Membr. Sci.* **2019**, *592*, 117372.

(15) Melchior, J.-P.; Jalarvo, N. H. A Quasielastic Neutron Scattering Study of Water Diffusion in Model Anion Exchange Membranes over Localized and Extended Volume Increments. *J. Phys. Chem. C* **2019**, *123* (23), 14195–14206.

(16) Dlugolecki, P.; Nymeyer, K.; Metz, S.; Wessling, M. Current Status of Ion Exchange Membranes for Power Generation from Salinity Gradients. *J. Membr. Sci.* **2008**, *319* (1–2), 214–222.

(17) FuelCellStore. Technical Data Sheet - Fumasep FAD-55. FuelCellStore. <https://www.fuelcellstore.com/fumasep-fad-55> (accessed November 18, 2019).

(18) Park, J.-S.; Choi, J.-H.; Woo, J.-J.; Moon, S.-H. An Electrical Impedance Spectroscopic (EIS) Study on Transport Characteristics of Ion-Exchange Membrane Systems. *J. Colloid Interface Sci.* **2006**, *300* (2), 655–662.

(19) Rezaei Niya, S. M.; Hoorfar, M. Study of Proton Exchange Membrane Fuel Cells Using Electrochemical Impedance Spectroscopy Technique – A Review. *J. Power Sources* **2013**, *240*, 281–293.

(20) Preen, M. A.; Woodward, J. D. Potentiometric Titration of Chloride in Beer and Wort Using an Ion-Selective Electrode. *J. Inst. Brew.* **1975**, *81* (4), 307–308.

(21) Northrop, J. A Convenient Method for Potentiometric Titration of Chloride Ions. *J. Gen. Physiol.* **1948**, *31* (3), 213–215.

(22) Metrohm. *Chloride Titrations with Potentiometric Indication, Application Bulletin 103/3 e*; pp 1–5.

(23) Chen, X.; Jiang, Y.; Yang, S.; Pan, J.; Yan, R.; Bruggen, B. V. der; Sotto, A.; Gao, C.; Shen, J. Internal Cross-Linked Anion Exchange Membranes with Improved Dimensional Stability for Electrodialysis. *J. Membr. Sci.* **2017**, *542*, 280–288.

(24) Kamcev, J.; Jang, E.-S.; Yan, N.; Paul, D. R.; Freeman, B. D. Effect of Ambient Carbon Dioxide on Salt Permeability and Sorption Measurements in Ion-Exchange Membranes. *J. Membr. Sci.* **2015**, *479*, 55–66.

- (25) Geise, G. M.; Freeman, B. D.; Paul, D. R. Sodium Chloride Diffusion in Sulfonated Polymers for Membrane Applications. *J. Membr. Sci.* **2013**, *427*, 186–196.
- (26) Xie, W.; Cook, J.; Park, H. B.; Freeman, B. D.; Lee, C. H.; McGrath, J. E. Fundamental Salt and Water Transport Properties in Directly Copolymerized Disulfonated Poly(Arylene Ether Sulfone) Random Copolymers. *Polymer* **2011**, *52* (9), 2032–2043.
- (27) Geise, G. M.; Freeman, B. D.; Paul, D. R. Characterization of a Sulfonated Pentablock Copolymer for Desalination Applications. *Polymer* **2010**, *51* (24), 5815–5822.
- (28) Kamcev, J.; Galizia, M.; Benedetti, F. M.; Jang, E.-S.; Paul, D. R.; Freeman, B. D.; Manning, G. S. Partitioning of Mobile Ions between Ion Exchange Polymers and Aqueous Salt Solutions: Importance of Counter-Ion Condensation. *Phys. Chem. Chem. Phys.* **2016**, *18* (8), 6021–6031.
- (29) Kingsbury, R. S.; Zhu, S.; Flotron, S.; Coronell, O. Microstructure Determines Water and Salt Permeation in Commercial Ion-Exchange Membranes. *ACS Appl. Mater. Interfaces* **2018**, *10* (46), 39745–39756.
- (30) Chang, K.; Xue, T.; Geise, G. M. Increasing Salt Size Selectivity in Low Water Content Polymers via Polymer Backbone Dynamics. *J. Membr. Sci.* **2018**, *552*, 43–50.
- (31) Yan, X.; Zhang, C.; Dai, Y.; Zheng, W.; Ruan, X.; He, G. A Novel Imidazolium-Based Amphoteric Membrane for High-Performance Vanadium Redox Flow Battery. *J. Membr. Sci.* **2017**, *544*, 98–107.
- (32) Dlugolecki, P.; Anet, B.; Metz, S. J.; Nijmeijer, K.; Wessling, M. Transport Limitations in Ion Exchange Membranes at Low Salt Concentrations. *J. Membr. Sci.* **2010**, *346* (1), 163–171.
- (33) FuelCellStore. Membranes <https://www.fuelcellstore.com/fuel-cell-components/membranes> (accessed Jul 24, 2019).
- (34) Stenina, I. A.; Sistat, Ph; Rebrov, A. I.; Pourcelly, G.; Yaroslavtsev, A. B. Ion Mobility in Nafion-117 Membranes. *Desalination* **2004**, *170* (1), 49–57.
- (35) Murata, K.; Irish, D. E.; Toogood, G. E. Vibrational Spectral Studies of Solutions at Elevated Temperatures and Pressures. 11. A Raman Spectral Study of Aqueous Iron(III) Chloride Solutions between 25 and 300 °C. *Can. J. Chem.* **1989**, *67* (3), 517–524.
- (36) Lee, M.-S.; Ahn, J.-G.; Oh, Y.-J. Chemical Model of the FeCl₃-HCl-H₂O Solutions at 25 °C. *Mater. Trans.* **2003**, *44* (5), 957–961.
- (37) Sitze, M. S.; Schreiter, E. R.; Patterson, E. V.; Freeman, R. G. Ionic Liquids Based on FeCl₃ and FeCl₂. Raman Scattering and Ab Initio Calculations. *Inorg. Chem.* **2001**, *40* (10), 2298–2304.
- (38) Marston, A. L.; Bush, S. F. Raman Spectral Investigation of the Complex Species of Ferric Chloride in Concentrated Aqueous Solution. *Appl. Spectrosc.* **1972**, *26* (6), 579–584.
- (39) Reiner, A.; Ledjeff, K. Anion Exchange Membranes Consisting of Poly (Vinylpyridine) and Poly (Vinylbenzyl Chloride) for Cr/Fe Redox Batteries. *J. Membr. Sci.* **1988**, *36*, 535–540.
- (40) Marcus, Y.; Kertes, A. S. Anion Exchange of Complexes. In *Ion Exchange and Solvent Extraction of Metal Complexes*; Wiley - Interscience: 1969, pp 359–424.
- (41) Helfferich, F. Ion-Exchange Equilibria Involving Complexing Agents. In *Ion Exchange*; McGraw-Hill Book Company, Inc.: 1962; pp 202–226.
- (42) Geise, G. M.; Paul, D. R.; Freeman, B. D. Fundamental Water and Salt Transport Properties of Polymeric Materials. *Prog. Polym. Sci.* **2014**, *39* (1), 1–42.
- (43) Kamcev, J.; Sujanani, R.; Jang, E.-S.; Yan, N.; Moe, N.; Paul, D. R.; Freeman, B. D. Salt Concentration Dependence of Ionic Conductivity in Ion Exchange Membranes. *J. Membr. Sci.* **2018**, *547*, 123–133.
- (44) Luo, T.; Abdu, S.; Wessling, M. Selectivity of Ion Exchange Membranes: A Review. *J. Membr. Sci.* **2018**, *555*, 429–454.
- (45) Schlenoff, J. B.; Rmaile, A. H.; Bucur, C. B. Hydration Contributions to Association in Polyelectrolyte Multilayers and Complexes: Visualizing Hydrophobicity. *J. Am. Chem. Soc.* **2008**, *130* (41), 13589–13597.
- (46) Yuchi, A.; Kuroda, S.; Takagi, M.; Watanabe, Y.; Nakao, S. Effects of the Exchange Capacity and Cross-Linking Degree on the Hydration States of Anions in Quantitative Loading onto Strongly Basic Anion-Exchange Resins. *Anal. Chem.* **2010**, *82* (20), 8611–8617.
- (47) Nightingale, E. R. Phenomenological Theory of Ion Solvation. Effective Radii of Hydrated Ions. *J. Phys. Chem.* **1959**, *63* (9), 1381–1387.
- (48) Bontha, J. R.; Pintauro, P. N. Water Orientation and Ion Solvation Effects During Multicomponent Salt Partitioning in a Nafion Cation Exchange Membrane. *Chem. Eng. Sci.* **1994**, *49* (23), 3835–3851.
- (49) Mañé, S.; Ramírez, P.; Tanioka, A.; Pellicer, J. Model for Counterion-Membrane-Fixed Ion Pairing and Donnan Equilibrium in Charged Membranes. *J. Phys. Chem. B* **1997**, *101* (10), 1851–1856.
- (50) Okada, T.; Harada, M. Hydration of Halide Anions in Ion-Exchange Resin and Their Dissociation from Cationic Groups. *Anal. Chem.* **2004**, *76* (15), 4564–4571.
- (51) Weiber, E. A.; Jannasch, P. Polysulfones with Highly Localized Imidazolium Groups for Anion Exchange Membranes. *J. Membr. Sci.* **2015**, *481*, 164–171.
- (52) Gutmann, V.; Baaz, M. Conductivity Measurements in Phosphorus Oxychloride. V. Iron(III) Chloride and Aluminum Chloride. *Monatshfte fuer Chemie* **1959**, *90*, 729–743.
- (53) Duan, Q.; Ge, S.; Wang, C.-Y. Water Uptake, Ionic Conductivity and Swelling Properties of Anion-Exchange Membrane. *J. Power Sources* **2013**, *243*, 773–778.
- (54) Berezina, N. P.; Kononenko, N. A.; Dyomina, O. A.; Gnusin, N. P. Characterization of Ion-Exchange Membrane Materials: Properties vs Structure. *Adv. Colloid Interface Sci.* **2008**, *139* (1–2), 3–28.
- (55) Geise, G. M.; Hickner, M. A.; Logan, B. E. Ionic Resistance and Permselectivity Tradeoffs in Anion Exchange Membranes. *ACS Appl. Mater. Interfaces* **2013**, *5* (20), 10294–10301.